ELSP elspublishing

OPEN ACCESS
Article

Surface subsidence patterns and mechanisms of underlying goaf beneath a railway tunnel

Haining Ma, Tianfeng Gu*, Bo Cui, Shuai Li, Yuxin Tang and Rongxuan Feng **E-mail:** gutf@nwu.edu.cn

Received 12 September 2025; Revised 16 November 2025; Accepted 8 January 2026; Published 2 March 2026
https://doi.org/10.55092/cle20260003

Graphical Abstract

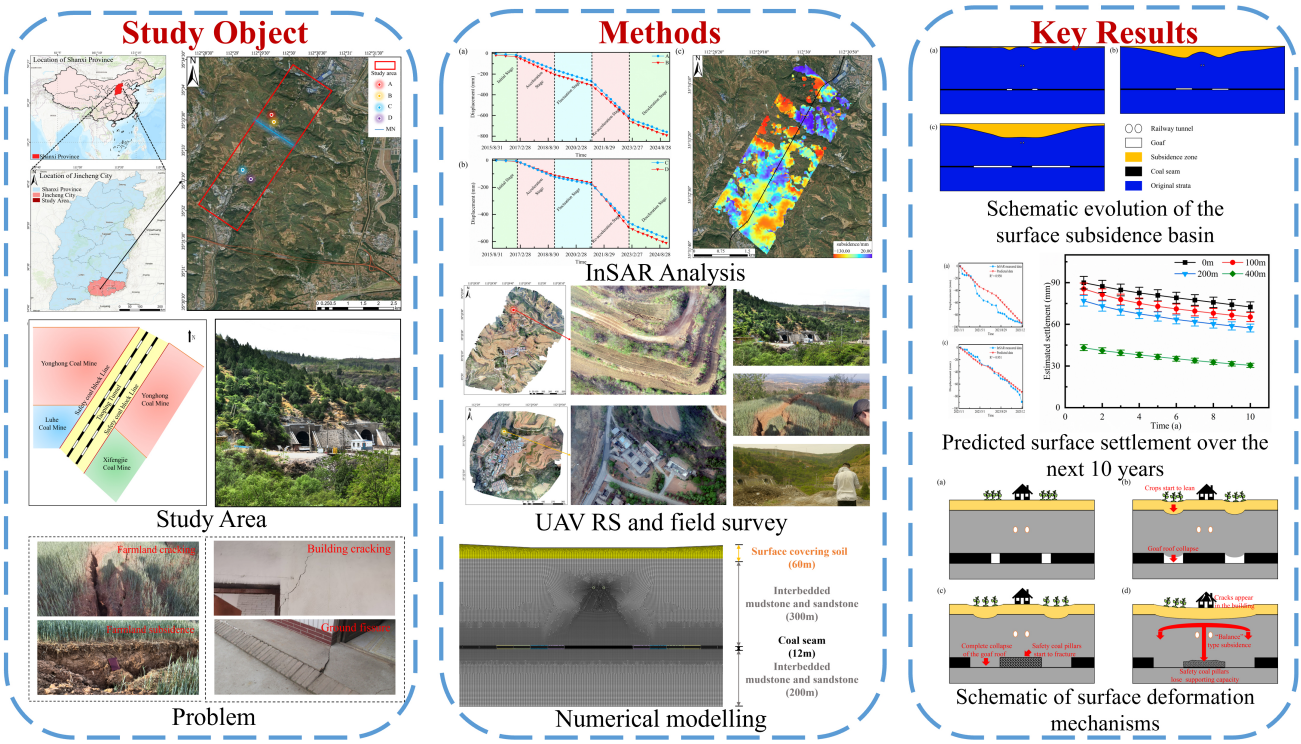

Highlights:

- Five-stage deformation sequence (2015–2024) revealed above the Taoping tunnel goaf; settlement continues > 10 years after mining ceased.
- Pillar progressive failure converts isolated local basin into a “Balance-type” instability structure, merging adjacent goafs.
- Time-series InSAR, numerical modelling and probability-integral method jointly quantify evolution and future residual settlement.
- Residual stabilization predicted within next 10 years, offering a predictive framework for railway safety and land reuse.

Surface subsidence patterns and mechanisms of underlying goaf beneath a railway tunnel

Haining Ma[1,2], Tianfeng Gu[1,2,*], Bo Cui[1,2], Shuai Li[1,2], Yuxin Tang[1,2] and Rongxuan Feng[1,2]

[1] Department of Geology, Northwest University, Xi'an 710069, China

[2] China-Kyrgyzstan Belt and Road Joint Laboratory on Special Geotechnical Dynamic Disaster Prevention and Control, Northwest University, Xi'an 710069, China

E-mail: gutf@nwu.edu.cn.

Abstract: Long-term deformation of abandoned mine workings endangers surface infrastructure, causing wall cracking, beam–column distortion and, in extreme cases, tilting or collapse. Here we track surface movement above the Taoping tunnel goaf beneath the Houyue railway (Shanxi, China) by combining 2015–2024 InSAR time-series, numerical modelling and probability-integral analysis. Contrary to widely held stability assumptions, subsidence is still accelerating more than a decade after extraction ceased. Five evolutionary stages are identified: (1) initial roof failure and local basin formation; (2) stress redistribution that loads the safety coal pillar; (3) progressive pillar crushing; (4) merger of adjacent goafs into a "balanced" instability structure; and (5) transformation of the local basin into a regional trough. Probability-integral forecasting indicates residual settlement will continue for roughly ten years before stabilization. The proposed stage-based framework enables long-term stability assessment and targeted remediation of similar legacy goafs, and supports safe railway operation and future land reuse.

Keywords: goaf; surface subsidence; InSAR; numerical modelling; subsidence mechanism

1. Introduction

China's extensive railway network has formed a large-scale pattern, with over 21,000 operational and under-construction tunnels as of 2024 (Gong *et al.* 2025). However, in mineral-rich regions such as Shanxi and Anhui provinces, numerous tunnels inevitably traverse goaf zones formed by mining, exposing such projects to significant risks including collapse and structural deformation. China's vast coal reserves have long underpinned its economic growth, yet large-scale extraction has simultaneously triggered extensive ecological and social challenges (Li *et al.* 2022). Mining disrupts the equilibrium of overlying strata: the upward propagation of stress from the seam causes caving, fracturing and flexural subsidence (Sun *et al.* 2019; Wo *et al.* 2022; Liu *et al.* 2024). Contrary to the widely accepted "mine-stabilize" paradigm, settlement above the Taoping tunnel goaf on the Houyue railway persists decades after extraction ceased. Continuous subsidence drives pronounced surface deformation, damages the surrounding geology and endangers sustainable land use and infrastructure safety (Zhu *et al.* 2024c). Accurate monitoring, analysis and prediction of this goaf subsidence are therefore essential. Although Chen (Chen 2025) and Wang (Wang 2025) concentrated on tunnel damage and settlement at the tunnel site, this study tracks the long-term evolution of surface subsidence above the goaf and clarifies the mechanisms that drive it. A key characteristic of this mining panel is its symmetric layout, with safety coal pillars acting as the axis of symmetry. This geometry sustains a residual stress imbalance that has produced conspicuous surface subsidence for more than thirty years after mining stopped, challenging traditional stability assumptions and demanding a clear mechanistic explanation.

Surface subsidence above mine goafs is governed by mining-induced stress redistribution, and is further conditioned by geological structure, groundwater flow and subsequent engineering works. These coupled factors create a nonlinear, stochastic subsidence field that evolves over decades. Identifying the underlying mechanisms therefore remains central to understanding mining-related geohazards (Herrera-García *et al.* 2021; Modeste *et al.* 2021). Traditional monitoring has relied on levelling and GNSS. Levelling delivers precise point measurements, yet demands intensive field crews is impractical for large-area, long-term monitoring (Declercq *et al.* 2023; Zhu *et al.* 2024*a*). GNSS networks avoid this manpower burden but achieve millimeter accuracy only where receiver quality and sky-view geometry are optimal (Yulaikhah *et al.* 2019; Hamza *et al.* 2024). Dense networks are required to capture spatial variability, causing equipment, installation and maintenance costs to rise nonlinearly (Wang *et al.* 2021). Consequently, both techniques struggle to resolve the full spatiotemporal complexity of goaf subsidence across regional scales. Since its first demonstration in 1989 (Zhu *et al.* 2024b), Interferometric Synthetic Aperture Radar (InSAR) has evolved into the reference method for mining-deformation mapping, validated by co-located GNSS observations (Apanowicz *et al.* 2025). Day-and-night, all-weather operation, sub-weekly revisit and millimetric precision have displaced traditional levelling networks over large areas (Gabriel *et al.* 1989; Wang *et al.* 2022). The two operational streams—Persistent Scatterer (PS) and Small Baseline Subset (SBAS) InSAR—are now routine: PS extracts coherent point targets to monitor slow residual settlement after mine closure (Przyłucka *et al.* 2022; Huang *et al.* 2024; Zhang *et al.* 2024), while SBAS

exploits distributed scatterers to map complete subsidence basins above goafs with more than an order-of-magnitude gain in sampling density and efficiency compared with densified levelling (Kopeć *et al.* 2022; Li *et al.* 2023; Ashraf *et al.* 2024; Teixeira *et al.* 2024). We close this gap by integrating PS and SBAS InSAR for the Taoping tunnel goaf, delivering (i) millimetric validation of long-term stability on legacy infrastructure and (ii) kilometer-scale, spatiotemporally continuous quantification of ongoing subsidence within one coherent processing scheme.

Long-term stability assessment of abandoned mine workings remains challenging because geological conditions, external stresses and other factors interact in complex, nonlinear ways (Yuan *et al.* 2025). Three complementary approaches—analytical solutions, physical modelling and numerical simulation—are used worldwide. Advances in computing power have made numerical methods particularly attractive because they are easy to implement and increasingly accurate (Jia *et al.* 2022; Zhang *et al.* 2023; Li *et al.* 2024). Finite-element models can couple stress, displacement and plasticity within a single framework, reproducing progressive pillar yielding, roof caving and surrounding rock deformation. Outputs such as stress concentrations, peak tensile/compressive strains and displacement magnitudes quantify the residual subsidence zone and allow engineers to evaluate safety margins and optimize protection measures for buildings, embankments and support structures (Ren *et al.* 2022; Yang *et al.* 2022; He *et al.* 2023; Xu *et al.* 2023; Guo *et al.* 2024). Goaf settlement can be divided into three phases: initial, active and residual. When analyzing residual subsidence, existing numerical simulations generally focus on rock-mass creep, geometric parameters of the goaf (burial depth, span, height and shape) and groundwater effects, while the time-dependent degradation of safety coal pillar strength is rarely incorporated (Salmi *et al.* 2017; Shi *et al.* 2020; Dudek *et al.* 2022; Jeon *et al.* 2022; Sidki-Rius *et al.* 2022; Sakhno *et al.* 2023; Zhou *et al.* 2023b). Taking the special spatial configuration of this goaf as the basis, in addition to considering the span of the void, this study is the first to introduce pillar-strength decay into the model. It is precisely the progressive failure of the pillar that sustains significant settlement after mining has ceased, offering a new perspective for analyzing similar residual subsidence problems. Polish scholar Litwiniszyn introduced stochastic medium theory in 1956 to describe strata movement (Litwiniszyn 1956); Liu Baochen *et al.* later derived the probability integral method (PIM) (Liu and Liao 1965). The PIM requires only a few physically meaningful parameters that are easily calibrated. When combined with InSAR and numerical results through joint inversion, it reduces the maximum absolute error between prediction and measurement and has become the standard tool for forecasting surface subsidence above abandoned workings in China (Jiang *et al.* 2019; Fan *et al.* 2021; Duan *et al.* 2023; Cong *et al.* 2024; Rigamonti *et al.* 2025). This study therefore integrates high resolution finite element modelling with PIM. The numerical model captures the complex goaf geometry and failure mechanisms, while the PIM provides a robust, validated prediction of surface settlement. Together, they improve both mechanistic understanding and forecasting accuracy.

Using Sentinel-1 imagery (2015–2024) and a joint PS–SBAS InSAR approach, we generated continuous surface deformation time series above the Taoping tunnel goaf. Complementary finite-element analyses quantified the influence of varying extraction lengths on surface settlement. Settlement persisted long after mining ceased, contradicting the traditional "mine-stabilize" paradigm. This prolonged subsidence is governed by the symmetric geometry of the goaf–pillar–goaf system. Progressive decay of pillar strength and associated rupture dictate the post extraction deformation pattern. The results provide a mechanistic basis for evaluating stability and designing remedial measures in similar goaf–tunnel settings, and scientific guidance for regional land reuse, tunnel safety and sustainable development.

2. Study area

The Taoping tunnel is located in the transition zone between Qinshui and Yangcheng counties, Jin-cheng City, Shanxi Province, in the moderately elevated terrain of southeastern Shanxi. It lies between Jiafeng and Yangcheng stations on the Houyue railway (Figure 1a). The project consists of two parallel, single track electrified tunnels at a depth of 145 m. The portal section crosses the Yonghong coalfield, where the seam is situated 200 m directly beneath the tunnel axis; the exit section borders the Xifengjie and Luhe collieries, with the seam 100 m below the tunnel axis (Tian and Wang 2022). A total of 20 goaf zones have been created within and adjacent to the alignment (Figure 1b) (Wang *et al.* 2019). The exploited seam dips 3–5° and averages 6.14 m in thickness. Its vertical distance from the tunnel invert ranges from 120 to 240 m (180 to 330 m below ground), giving depth to thickness ratios of 20.4–38.3. Continuous extraction occurred from 1992 to 2016 and resumed from 2021 to 2023. To safeguard long-term tunnel operation, safety coal pillars were deliberately retained beneath the tunnel. These pillars act as critical load-bearing elements that control surface deformation; their symmetrical arrangement with the pre-existing goaf governs the spatiotemporal evolution of regional subsidence.

The region is structurally simple: sub-horizontal strata form a broad, gentle syncline flanked by a secondary anticline. Tectonic drag has created dense jointing and fracturing, leaving the rock mass highly fragmented and weak. The sequence consists mainly of Permian sandstone interbedded with mudstone. Groundwater occurs as fissure water in the bedrock, recharged chiefly by precipitation and secondarily by surface water bodies. The dense joints and fractures, together with the fissure water with in the rock mass, pose a significant safety hazard and may further trigger collapse of the goaf (Zhang 2009).

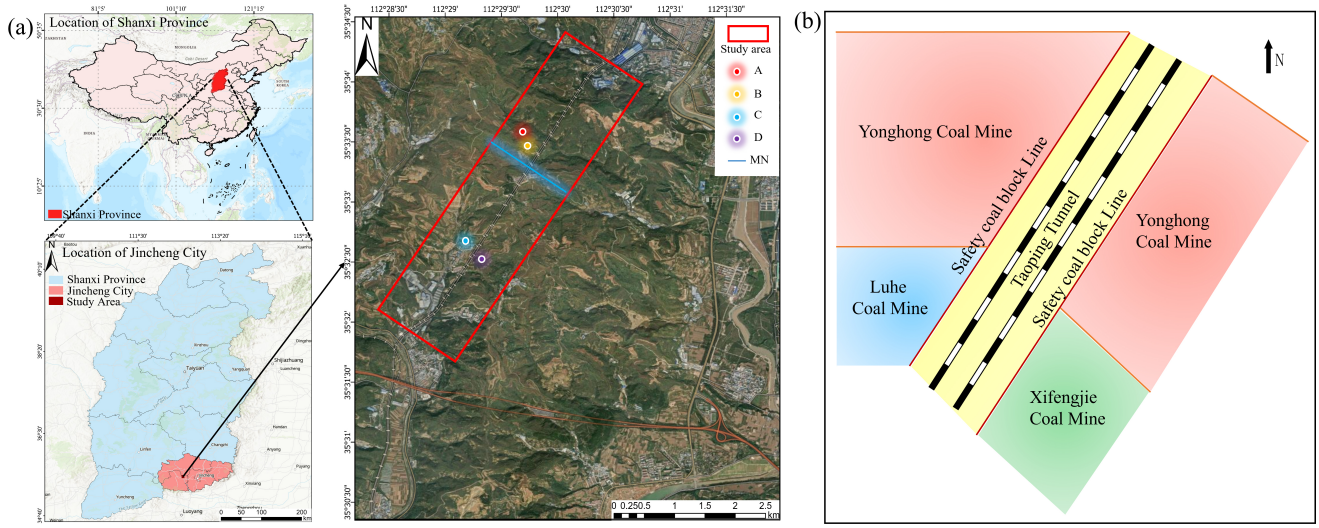

Figure 1. Study area location: **(a)** geographical setting; **(b)** spatial relationship between the tunnels and adjacent mine goafs.

Unmanned-aerial-vehicle (UAV) imagery and surface reconnaissance were used to document geohazards above the Taoping tunnel goaf. Owing to safety restrictions, only surface surveys were conducted. Observed damage includes ground collapses and cracking of buildings and roads near the tunnel. Figure 2a: Cropland in Goubei Village. Residents reported continuous subsidence that culminated in March 2025 with the formation of a sink-like depression 0.5 m wide and 1.0 m deep; cultivation is now impossible in the affected area. Figure 2b: Residential structure in Taoping Village. Both the foundation and interior walls show activity. Moreover, previous studies reveal that well developed ground fissures and building cracks are also present in the center of the subsidence basin (Wang *et al.* 2019). Widening fractures threaten structural integrity and pose immediate risks to life and property.

Taoping tunnel deterioration unfolded in four stages: From 1996 to 1999 (Initial)—Multiple cracks appeared in the upline lining. From 2004 to 2013 (Intensification)—Severe vertical cracks formed in both sidewalls of the upline portal, accompanied by crown cracking and spalling. Between 4 September and 16 October 2006, the downline tunnel experienced 22 block fall events, a continuous longitudinal crown fracture, crushing, spalling and local bulging, cracking and benching of the right side wall. From 2013 to 2017 (Rapid deterioration)—On 9 May 2013, new distress emerged at the north ends of both tunnels: horizontal, 45° diagonal, and circumferential cracks, lining bulging and uplift and crushing with block fall at the haunches. On 9 December 2014, the downline lining again suffered detachment and block fall. From 2017 to the present (Ongoing)—Continuous surface deformation and cracking have been observed above the tunnels (Li 2019).

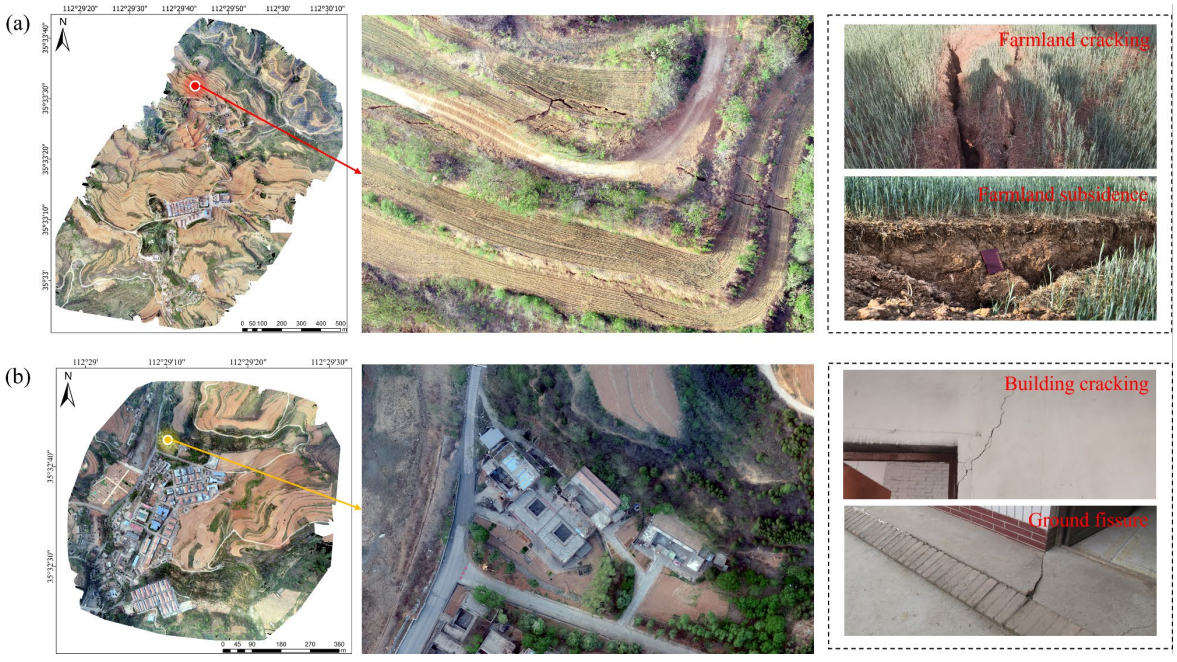

Figure 2. UAV imagery and field survey: **(a)** Dafujie Village; **(b)** Taoping Village.

3. Theory for data processing

3.1. InSAR monitoring data selection and processing

The subsidence magnitudes above the Taoping tunnel goaf are small, yet fall well within the millimeter-level sensitivity of InSAR. By analyzing phase differences among multi-temporal SAR images, displacements can be recovered with sub-centimeter accuracy. To suppress decorrelation and atmospheric artefacts under complex land cover conditions, we applied PS-InSAR and SBAS-InSAR in parallel. For both approaches, interferograms were generated only for image pairs with a temporal baseline ≤ 365 days and a perpendicular spatial baseline ≤ 45% of the critical baseline. Phase unwrapping was performed with the Goldstein branch cut algorithm, adopting an unwrapping correlation threshold of 0.20; pixels were retained if their correlation coefficient exceeded 0.30, while the final coherence mask required an average coherence ≥ 0.75. PS-InSAR exploits persistent scatterers for phase stable observations, whereas SBAS uses the above spatiotemporal baseline constraints followed by singular value decomposition to jointly solve multi-master interferograms (Zhang *et al.* 2024). The two methods cross-validate each other, yielding a high-precision deformation time series for 2015–2024. We selected 245 ascending Sentinel-1A images acquired between May 2015 and December 2024 (data gap: June–September 2016). Precise Orbit Determination (POD) products from ESA refined the orbital state vectors, and the 12.5 m resolution ALOS World 3D DEM from JAXA removed topographic phase residuals. Satellite parameters are summarized in Table 1.

Table 1. Satellite parameters.

SAR Sensor Parameters	Operational Period	Repeat Cycle/Days	Operating Band (Wavelength/cm)	Polarization Mode
ALOS	January 2006 –May 2011	46	L (23.5)	HH
Sentinel-1A	April 2014–present	12	C (5.63)	HV

3.2. Numerical model establishment

To thoroughly investigate the potential impact of goaf deformation on the tunnel, a two-dimensional numerical model 2000 m long and 572 m high (Figure 3) was constructed using Midas GTS NX.

The stratigraphic column was simplified into four layers: 60 m of overburden, 300 m of interbedded mudstone–sandstone above the seam, a 12 m thick coal seam and 200 m of interbedded mudstone–sandstone below. All layers were represented by a modified Mohr–Coulomb model; parameters (Table 2) were obtained from site investigations and the literature (Wang 2025). Model boundaries were fixed laterally and at the base, with the constraint implemented as an automatic normal-displacement fix to reproduce *in-situ* conditions; gravitational body forces and realistic tunnel loads were then applied.

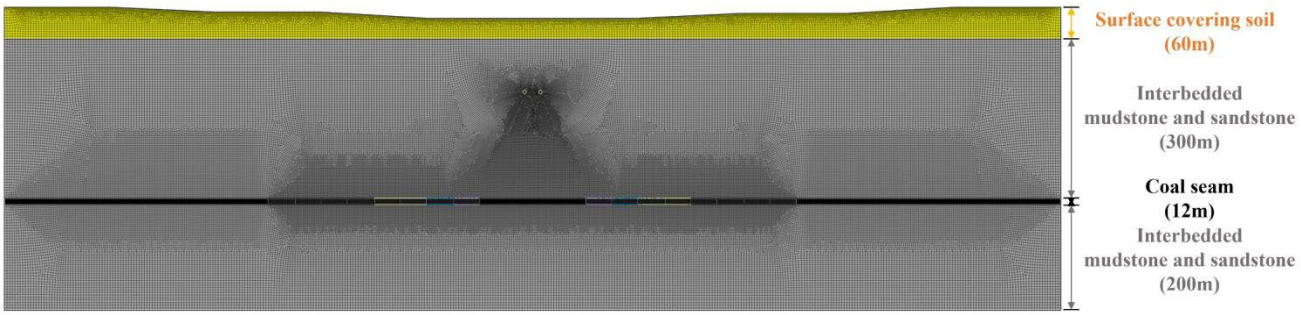

Figure 3. Goaf numerical model.

Table 2. Basic parameters of model materials.

Type	Compression Modulus/kPa	Poisson's Ratio	Cohesion/kPa	Internal Friction Angle/°
Surface overburden	1.0×10^4	0.30	15	18
Mudstone–sandstone alternation	1.5×10^6	0.19	1500	33
Coal seam	5.0×10^5	0.36	1000	25

3.3. Probability-integral method considering creep

After a goaf forms, stress redistribution occurs in the surrounding rock. This redistribution drives strata movement and, ultimately, leads to surface subsidence. The PIM—a widely used tool for predicting mining-induced deformation—treats the rock mass as a stochastic medium composed of infinitesimal elements (Peng *et al.* 2021; Du *et al.* 2025; Zhou *et al.* 2025). Specifically, the extraction of each element contributes a point source displacement. By integrating

these individual contributions, the cumulative surface subsidence profile can be derived. The governing equations are as follows:

$$W_{\max} = \int_0^L \frac{q \bullet \sqrt{1+(\frac{H_0}{r})^2}}{1+\frac{H_0}{r}} dL \quad (1)$$

where W_{max} = maximum surface subsidence, L = horizontal projection length of the mine goaf, q = subsidence coefficient, H_0 = depth to the goaf and r = principal influence radius.

Given the Taoping tunnel goaf's deep burial and overlay by high-strength bedrock, a creep coefficient is incorporated into the PIM to predict long-term settlement (Jing *et al.* 2018). The vertical displacement at any surface point is then calculated as follows:

$$W(x) = \int_0^{W_{\max}} \frac{\pi}{4} \bullet \frac{1}{\sqrt{1+(\frac{x}{r})^2}} dW_{\max} \times K \quad (2)$$

where K = creep coefficient.

To model the visco-elastic–visco-plastic response of the overburden rock mass above the mine goaf, we adopt a Burgers model. Under uniaxial compression, its creep compliance is expressed as:

$$J(t) = \frac{1}{E_1} + \frac{t}{\eta_1} + (\frac{1}{E_2})(1-e^{\frac{-t}{\tau_2}}) \quad (3)$$

where E_1 = instantaneous elastic modulus, E_2 = Kelvin modulus, η_1 = vis-cosity coefficient and τ_2 = retardation time.

For deep-seated mine goafs, the steady-state creep term dominates the deformation behavior. Consequently, the ultimate creep compliance is defined as the limit when t → ∞:

$$J_\infty = \frac{1}{E_1} + \frac{1}{E_2} \quad (4)$$

Hence, the following is true:

$$K = \frac{J_\infty}{J_0} = \frac{\frac{1}{E_1}+\frac{1}{E_2}}{\frac{1}{E_1}} = 1+\frac{E_1}{E_2} \quad (5)$$

4. Results and discussion

4.1. InSAR-based surface deformation analysis

Four representative PS points (A, B, C, D in Figure 1) were selected in Dafujie and Taoping villages to track goaf-related surface deformation. UAV imagery and field surveys guided point placement; the resulting time-series curves are shown in Figure 4a,b, and mean deformation rates for the four PS points are listed in Table 3.

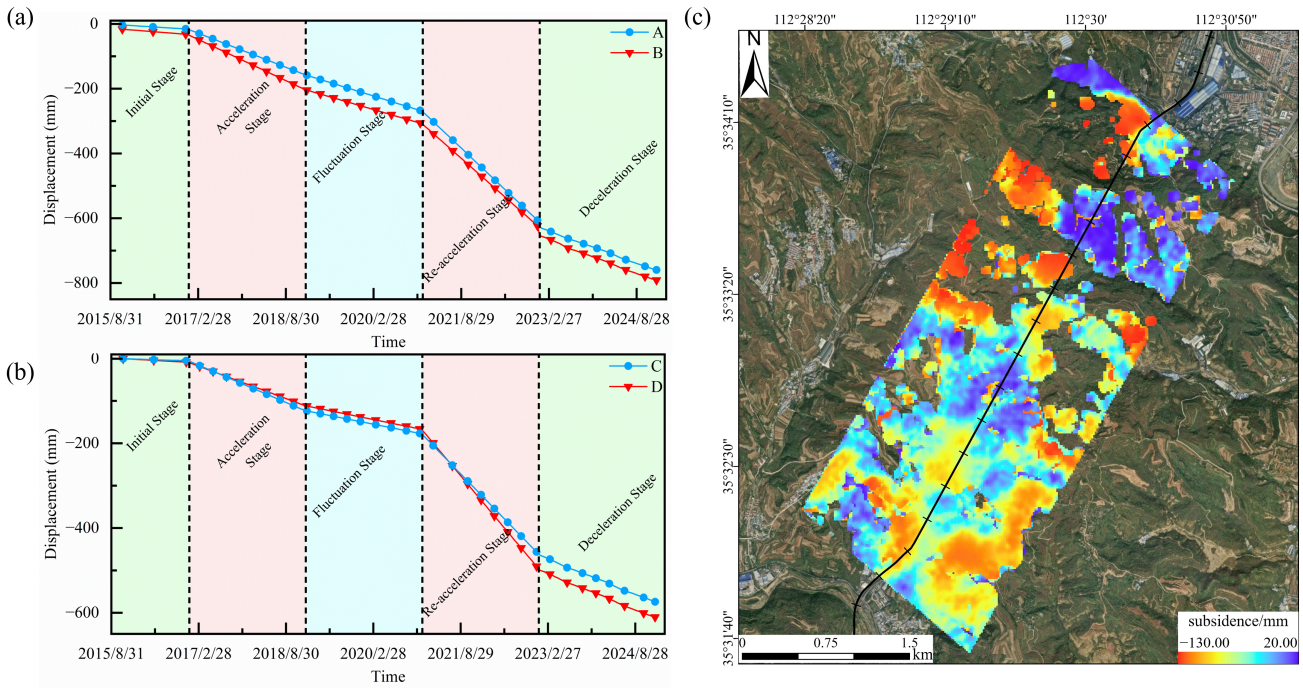

Figure 4. InSAR-derived results: **(a)** PS time series for points A and B; **(b)** PS time series for points C and D; **(c)** SBAS cumulative deformation map.

Table 3. Mean annual subsidence rates at monitoring points A–D across five deformation stages.

Stage	A (mm yr^{-1})	B (mm yr^{-1})	C (mm yr^{-1})	D (mm yr^{-1})
Initial stage (2015–2017)	−10.1	−8.3	−6.0	−3.2
Acceleration stage (2017–2018)	−58.4	−51.4	−40.5	−43.6
Fluctuation stage (2018–2020)	−36.2	−41.0	−22.1	−20.3
Re-acceleration stage (2020–2023)	−110.0	−125.0	−130.0	−105.0
Deceleration stage (2023–2024)	−93.5	−90.8	−87.5	−80.1

PS-InSAR indicates five distinct stages of subsidence above the Taoping tunnel goaf (2015–2024): (1) Initial (2015–2017): Flat curves; mean rate ≈ −4.3 mm yr^{-1}. The newly formed goaf loads the roof below its ultimate capacity; we therefore infer the rock mass remains intact, resulting in near-zero surface settlement. (2) Acceleration (2017–2018): Slope steepens sharply; rate jumps to ≈ −49.7 mm yr^{-1}. We attribute this to lateral expansion of the mined-out area, which increases the bending moment in the roof beam; the resulting beam rupture and collapse transmit stress waves to the surface, triggering rapid settlement. (3) Fluctuation (2018–2020): Slope flattens; rate moderates to ≈ −24.9 mm yr^{-1} yet stays negative. This is tentatively linked to complete roof caving and progressive compaction of the caved zone, leading to stress redistribution and decelerating, oscillatory subsidence. (4) Second acceleration (2020–2023): Slope increases again; rate peaks at ≈ −117.5 mm yr^{-1}. During this stage, the mine resumed extraction. We surmise the central safety pillar became the sole support; continued loading induced shear–splitting failure, and once its residual strength dropped below the critical threshold, stress release triggered renewed rapid settlement. (5) Deceleration (2023–2024): Slope declines; rate eases to ≈ −88.0 mm yr^{-1} while remaining negative. This is presumed to reflect stabilization of the pillar's residual strength and re-equilibration of the overlying rock mass, resulting in monotonic decay of the settlement rate.

The deformation-rate cross-section along profile MN (Figure 1a) is roughly symmetrical about the 1000 m mark (Figure 5), directly above the safety coal pillar. From 2015 to 2023, cumulative settlement increases monotonically, with substantially larger subsidence over the goaf than over the pillar. We attribute this pattern to progressive compaction and fracturing of the pillar fabric under sustained overburden and adjacent goaf influence, leading to continuous loss of bearing capacity. After 2021, marked additional settlement appears above the pillar, and its settlement rate converges toward that of the flanking goaf.

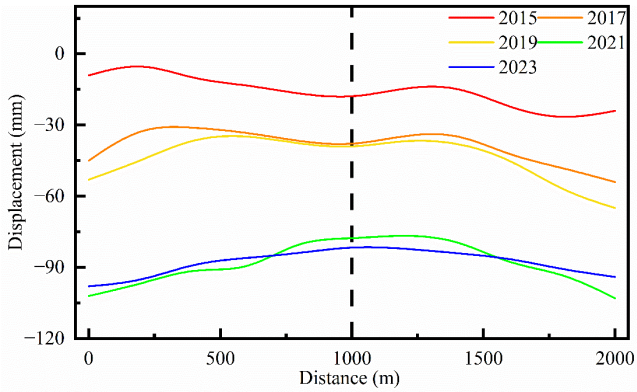

Figure 5. Deformation rate cross-section profile.

SBAS yielded a complete 2015–2024 deformation sequence, shown in Figure 4c. Subsidence along the Taoping tunnel alignment is strongly differential: symmetric funnels straddle the tunnel axis, with annual cumulative displacements ranging from −130.4 mm (settlement) to +10.3 mm (heave). The broad subsidence zone is centered above the goaf areas on both sides of the tunnel, in agreement with both field observations and PS-InSAR results.

SBAS derived deformation fields for Dafujie, Goubei and Taoping villages were extracted for 2015, 2017 and 2023 and cross-validated against contemporaneous PS-InSAR measurements; excellent agreement in both magnitude and trend were achieved (Figure 6). Peak subsidence evolved as follows: Dafujie: 30.0 mm (2015) → 69.9 mm (2017) → 96.3 mm (2023); Goubei: 17.0 mm (2015) → 77.5 mm (2017) → 92.4 mm (2023); Taoping: 17.9 mm (2015) → 42.7 mm (2017) → 93.5 mm (2023). Spatially, the loci of maximum settlement align closely with the goafs flanking the railway, and the same zones coincide with extensive farmland. Previous studies have shown that seasonal irrigation can induce shallow-layer consolidation settlement (Zhang *et al.* 2021; Cui *et al.* 2025). In the present area, irrigation enhanced subsidence is superimposed on mining induced collapse, jointly amplifying differential surface settlement.

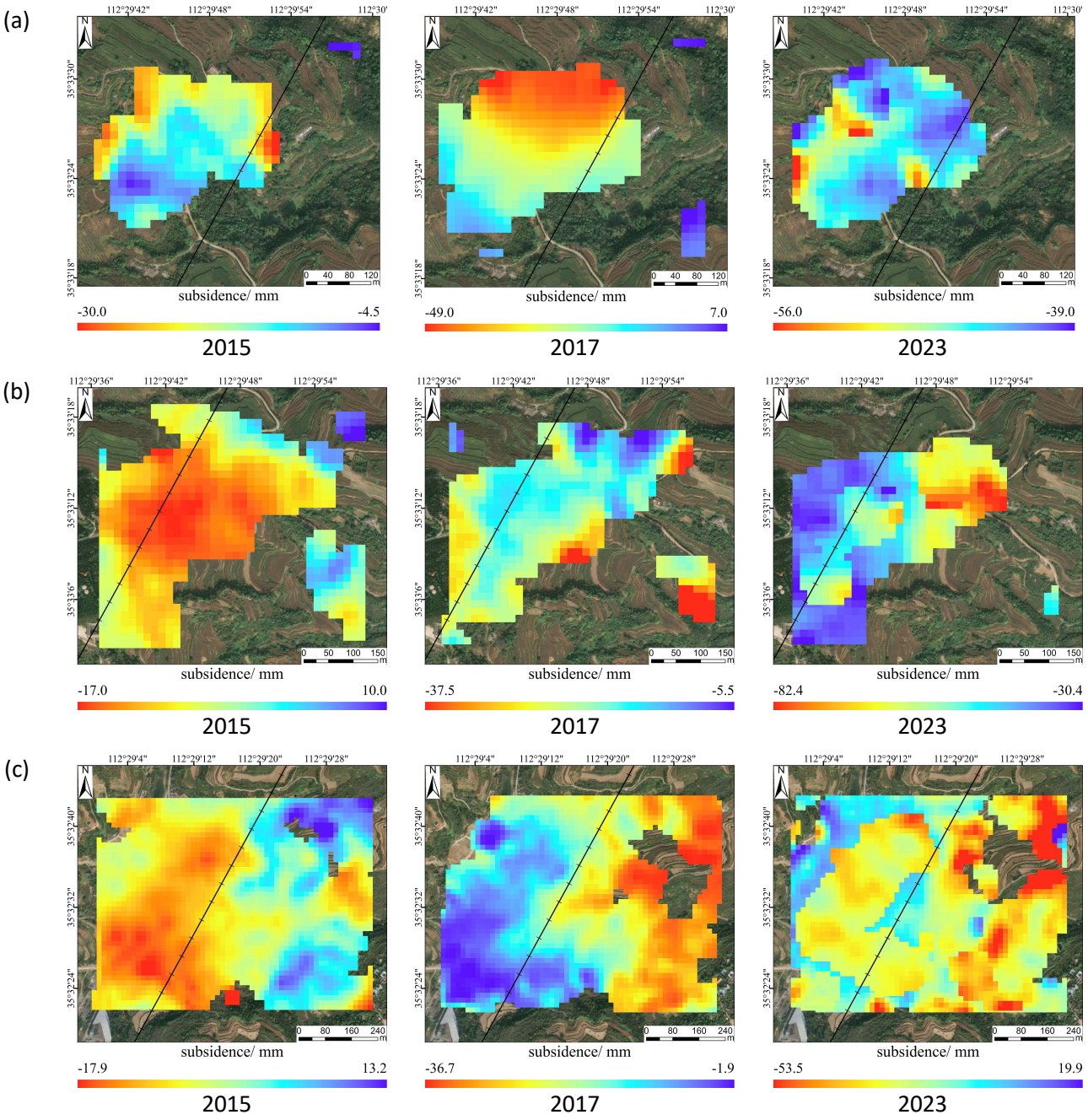

Figure 6. SBAS deformation maps for: **(a)** Dafujie Village; **(b)** Goubei Village; **(c)** Taoping Village.

4.2. Analysis of numerical simulation and probability-integral method results

4.2.1. Stress field analysis

To clarify the stress redistribution that follows coal extraction, we simulated the evolution of stress within the surrounding rock for eight goaf lengths—50, 100, 150, 200, 250, 300, 350 and 400 m—and examined stress concentrations at the goaf edges and within the safety pillar (Figure 7 and Figure 8). Mining disrupts the initial stress equilibrium (Figure 7a); the rock mass redistributes stresses to regain balance, producing pronounced local stress concentrations (Figure 7c). When these concentrations exceed rock-mass strength, damage and deformation develop (Figure 7d), ultimately triggering goaf instability.

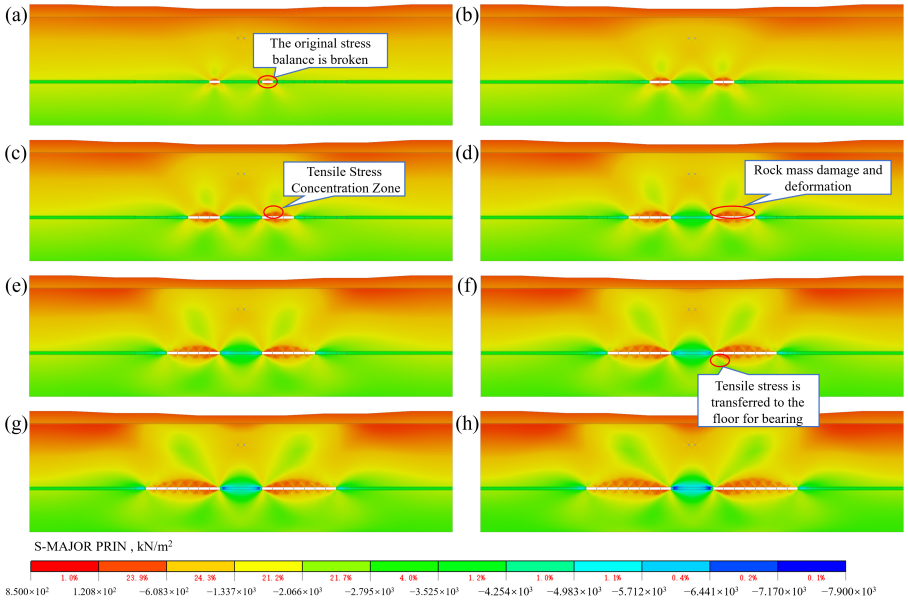

Figure 7. Tensile stress contour: **(a)** Excavation at 50 m; **(b)** Excavation at 100 m; **(c)** Excavation at 150 m; **(d)** Excavation at 200 m; **(e)** Excavation at 250 m; **(f)** Excavation at 300 m; **(g)** Excavation at 350 m; **(h)** Excavation at 400 m.

The stress contours reveal that, once the goaf is formed, the immediate roof and floor rapidly unload in vertical stress and undergo pronounced stress release owing to the loss of original rock support. Concurrently, tensile stress concentrations develop along the goaf periphery, generating high-stress-gradient zones. Along the goaf-adjacent side of the safety coal pillar, stress redistribution markedly alters the stress field, resulting in pronounced compressive stress concentration (Figure 8d). The stress patterns exhibit near symmetry, and this trend is consistently reproduced across all mining stages. As the goaf length increases, the extent of stress release in the roof and floor intensifies, and tensile stress magnitudes rise monotonically. Within the central safety coal pillar, compressive stress continuously accumulates with increasing extraction length (Figure 9). When these stresses reach or exceed the coal's compressive strength, the pillar suffers excessive loading, leading to crushing, deformation and ultimately rupture (Figure 8f). Because the Taoping tunnel is located directly above this retained coal seam, pillar deformation will inevitably propagate to the ground surface and induce corresponding deformation in the tunnel structure.

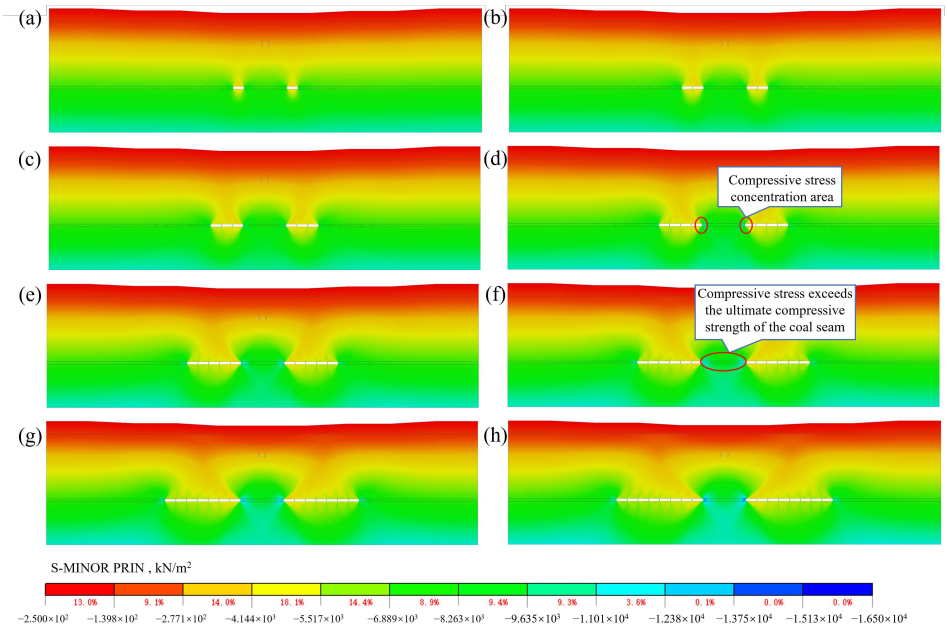

Figure 8. Tensile stress contour: **(a)** Excavation at 50 m; **(b)** Excavation at 100 m; **(c)** Excavation at 150 m; **(d)** Excavation at 200 m; **(e)** Excavation at 250 m; **(f)** Excavation at 300 m; **(g)** Excavation at 350 m; **(h)** Excavation at 400 m.

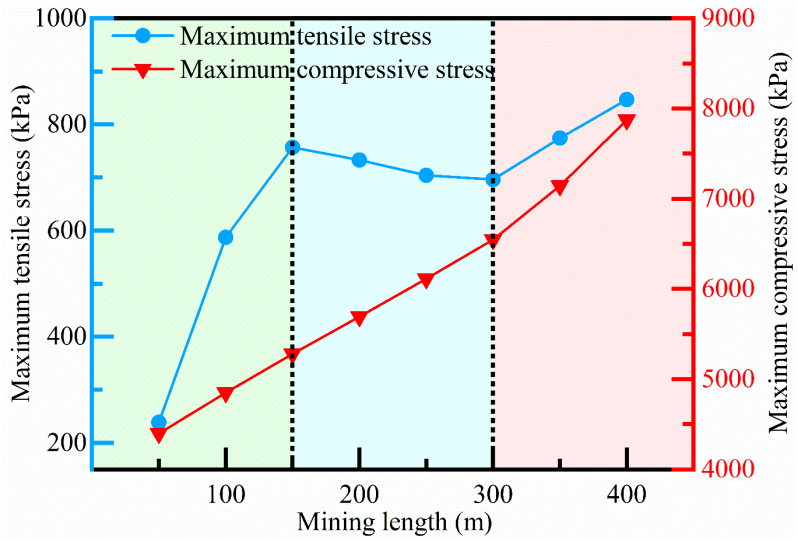

Figure 9. Variation in maximum tensile stress with extraction length.

After goaf formation, the immediate roof and floor rapidly lose vertical support and undergo pronounced stress release. Concurrently, tensile stress concentrations develop along the goaf periphery, creating steep stress gradients. Along the pillar side adjacent to the goaf, stress redistribution produces a marked compressive stress con-centration (Figure 8d); the pattern is nearly symmetrical and consistent across all simulated mining lengths. As the goaf lengthens, the area and magnitude of stress release in the roof and floor increase monotonically, and tensile stresses continue to rise. Compressive stress within the central safety pillar also accumulates progressively (Figure 9). When these stresses reach or exceed the coal's compressive strength, the pillar experiences crushing, deformation and eventual rupture (Figure 8f). Because the Taoping tunnel lies directly above the retained seam, pillar failure will propagate to the surface and induce corresponding deformation in the tunnel.

The goaf-adjacent stress field evolves in three distinct stages:

(a) Initial (0–150 m): As the face advances, the roof loses support and vertical stress is rapidly unloaded; a tensile zone develops and peaks in the roof, making it the region of maximum tension.

(b) Roof caving (150–300 m): When tensile stress exceeds the rock-mass tensile strength, the roof fractures and caves, eliminating the original tensile zone. Stress redistribution creates a new tensile concentration in the mid-floor; the locus of maximum tension thus migrates downward (Figure 10).

(c) Floor adjustment (> 300 m): Further span increase causes pronounced floor flexure. Tensile stress on the floor's lower surface rises monotonically; beyond 350 m, floor tensile stress continues to climb and is accompanied by slow settlement, indicating that the floor strata have entered a new progressive destabilization phase.

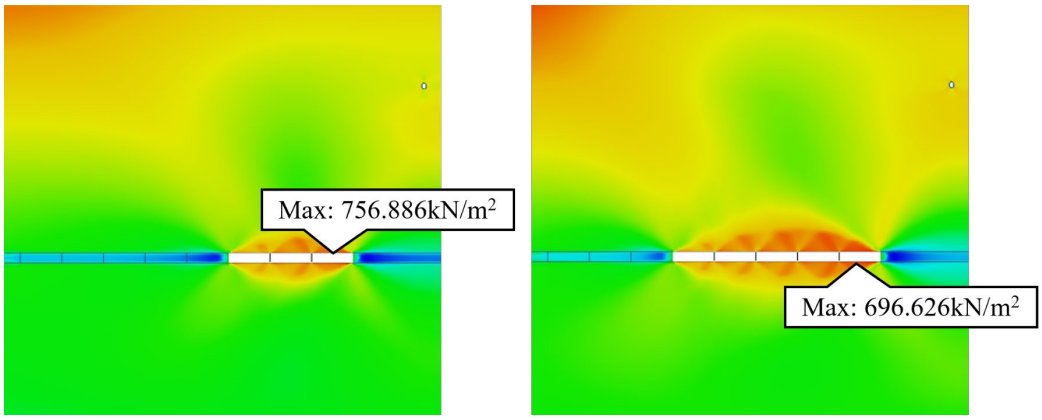

Figure 10. Schematic diagram of maximum tensile stress location migration.

4.2.2. Displacement analysis

Coal extraction inevitably deforms the surrounding rock. Displacement concentrates in the strata directly above the goaf and is almost entirely vertical; horizontal components are negligible. Contour maps for each extraction length (Figure 11) show a pronounced, symmetric pattern that mirrors the regular spatial influence of the goaf. These results were used to construct the schematic evolution of the surface subsidence basin shown in Figure 12.

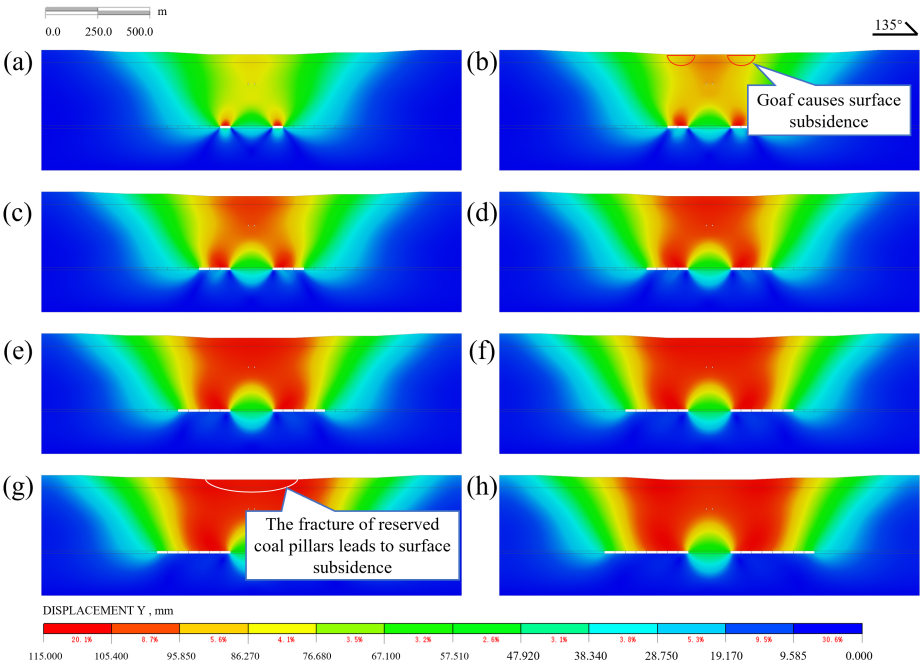

Figure 11. Displacement contour of goaf excavation: **(a)** Excavation at 50 m; **(b)** Excavation at 100 m; **(c)** Excavation at 150 m; **(d)** Excavation at 200 m; **(e)** Excavation at 250 m; **(f)** Excavation at 300 m; **(g)** Excavation at 350 m; **(h)** Excavation at 400 m.

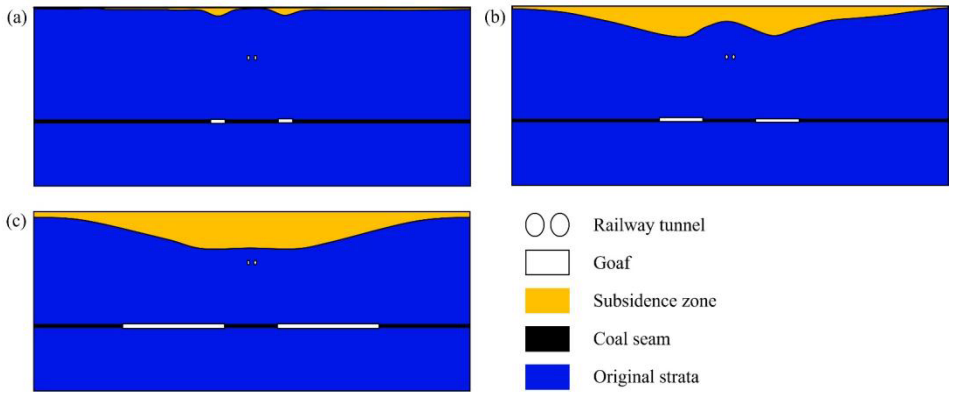

Figure 12. Schematic evolution of the surface subsidence basin: **(a)** Excavation at 50 m; **(b)** Excavation at 150 m; **(c)** Excavation at 350 m.

As the goaf span increases, roof movement propagates upward. Initially, a small, symmetric basin forms above the goaf center (Figure 11b and Figure 12b). Once the span is sufficient to trigger failure of the safety coal pillar, the pattern shifts from a local basin to a large-scale trough (Figure 11g and Figure 12c).

Numerical results show that the greatest vertical displacement always occurs at the center of the goaf roof, where strata have lost support. Displacement decreases steadily upward, creating a clear gradient from roof to surface (Figure 13). Both maximum roof displacement and final surface subsidence rise monotonically with extraction length, following a strong positive trend. This behavior aligns with the progressive key stratum fracture mechanism (Zhang *et al.* 2025): once the goaf length surpasses the critical span of the key stratum, successive failure of higher beams drives the subsidence basin outward, continuously enlarging the affected area and the magnitude of surface deformation.

To validate the numerical model, we compared the simulated displacements with InSAR measurements (Figure 14).

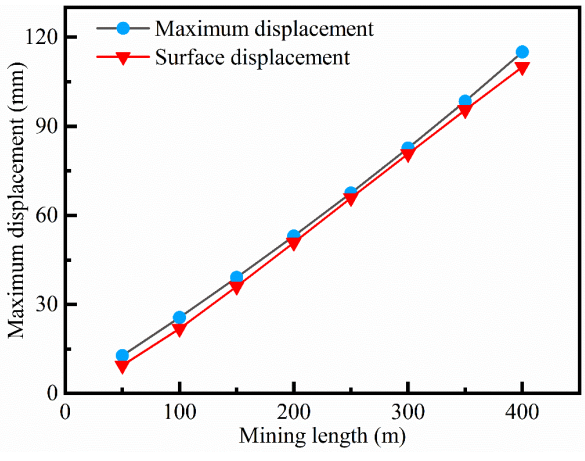

Figure 13. Vertical displacement versus mining length.

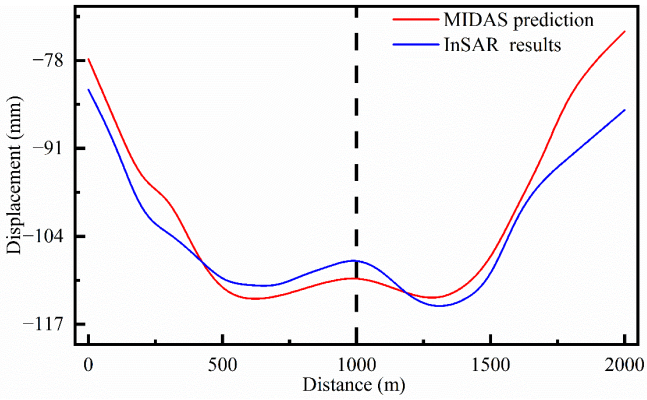

Figure 14. Comparison of numerically predicted surface deformation with InSAR measurements.

Model accuracy was evaluated with error metrics; percentage errors in maximum subsidence are listed below:

$$\mathrm{MRE} = \frac{1}{n}\sum_{i=1}^{n}\left|\frac{S_i - O_i}{O_i}\right| \times 100\% = 3.3\% \qquad (6)$$

where S_i is the simulated results and O_i is the measured results.

Since O_i = 3.3%, the MIDAS simulation results agree well overall with the InSAR-measured subsidence. Convergence is assessed using the L2 (Euclidean) norm of the normalized residual as follows:

$$\varepsilon = \frac{\|r\|_2}{\|R\|_2} \qquad (7)$$

where r is the unbalanced force vector and R is the external load vector.

All load steps satisfied $\varepsilon < 1 \times 10^{-3}$, with the final step converging to $\varepsilon = 7.30 \times 10^{-4}$, confirming that the numerical solution is stable and meets the required accuracy.

4.3. Settlement prediction

The probability-integral method is valid for gently inclined or near-horizontal seams (dip < 10°). With a seam dip of 3–5°, the Taoping tunnel area meets this criterion, so the creep-corrected PIM (Equation (2)) was adopted. The model was validated by nonlinear regression of InSAR time-series data from monitoring point A (2021–2024), as shown in Figure 15.

The coefficient of determination exceeds 0.95, confirming the model's reliability. Minor discrepancies arise because the adopted rock-mass parameters do not fully capture *in situ* heterogeneity, yet the error remains within acceptable limits and does not alter the overall conclusions. Using this validated model, we predicted surface settlement for the next decade at points located 0 m, 100 m, 200 m and 400 m from the goaf boundary along the dip direction (Figure 16).

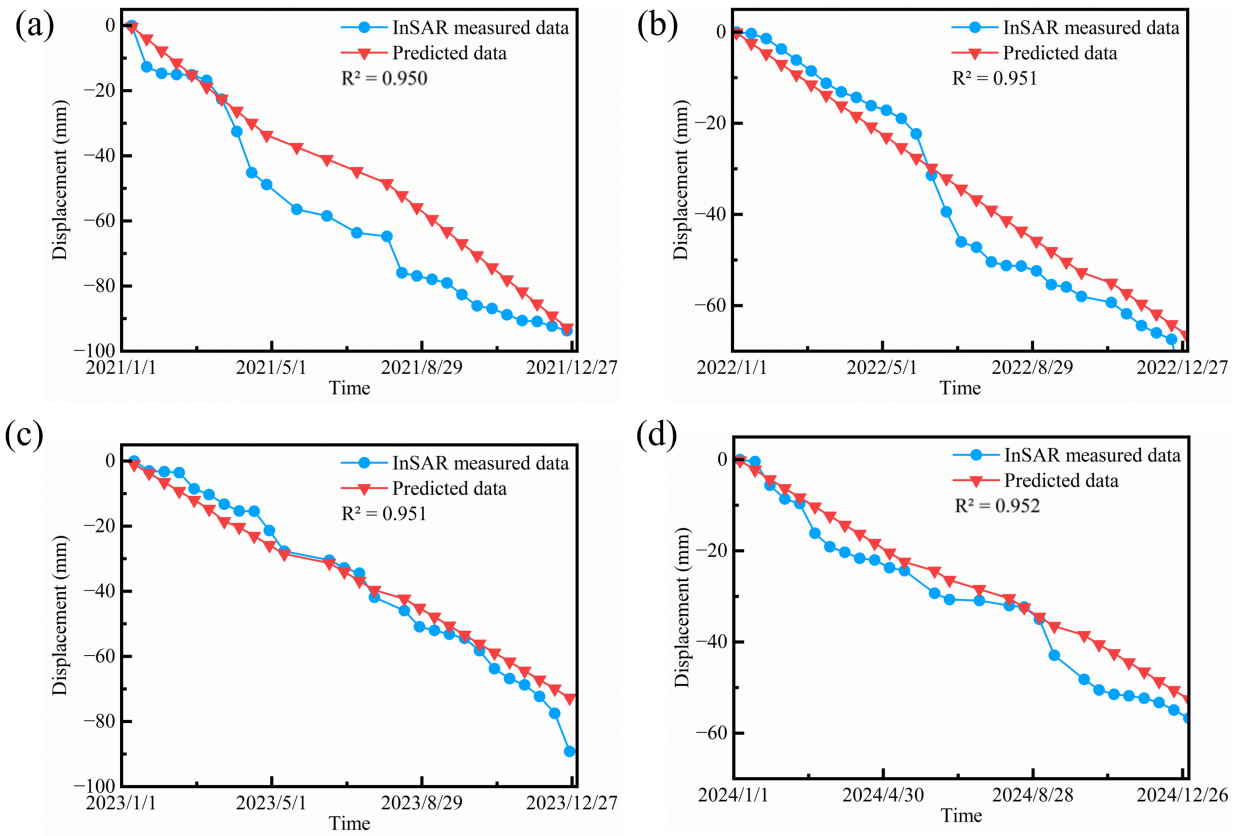

Figure 15. Model calibration results: **(a)** 2021; **(b)** 2022; **(c)** 2023; **(d)** 2024.

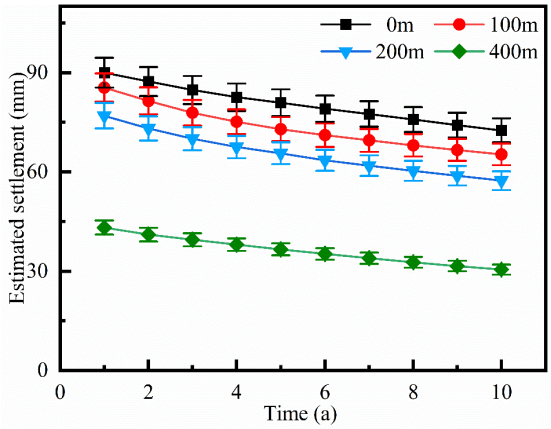

Figure 16. Predicted surface settlement over the next 10 years at selected locations above the goaf, with vertical error bars representing 95%.

Forward modelling for the next decade shows two clear patterns. Spatial decay: Settlement decreases monotonically with distance from the goaf center—90 mm in year 1 at the center (0 m) falls to 43.2 mm at 400 m. Temporal decay: Annual settlement declines progressively; by year 10, cumulative values drop to 72.5 mm at the center and 30.5 mm at 400 m. The rapid attenuation with distance and the convergent trend indicate that the Taoping tunnel goaf is entering the residual stabilization phase.

4.4. Deformation mechanism analysis

Goaf formation beneath the Taoping tunnel is a coupled, progressive process in which stress redistribution, deformation and failure interact continuously. Integrating InSAR, numerical modelling and theory, we infer this evolution into four stages (Figure 17):

(a) Initial—Extraction begins; the domain remains stable, bending moments are low, and only millimeter-scale displacements occur. No measurable surface movement is detected.

(b) Goaf influence—As the panel lengthens, thick roof beams fail in combined bending and tension. Roof collapse initiates and a local subsidence basin forms.

(c) Safety-pillar crushing—Continued collapse transfers the entire overburden to the central safety pillars, which become isolated load-bearing "islands". When axial stress exceeds the coal's capacity, the pillars crush, causing rapid surface settlement above them.

(d) Integrated interaction—Progressive pillar disintegration and lateral goaf expansion eliminate effective support. A symmetric "Balance" type unstable structure develops: large bowls flank the goaf while a smaller trough forms above the remnants of the pillars. Surface deformation shifts from isolated basins to a single, large-scale trough.

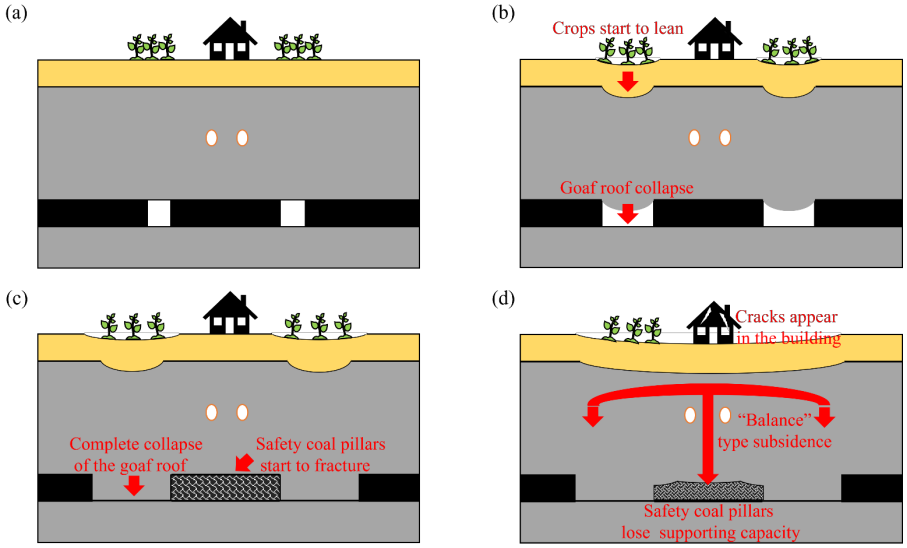

Figure 17. Schematic of surface deformation mechanisms above the Taoping tunnel goaf: **(a)** Initial stage; **(b)** Goaf-influence stage; **(c)** Safety-pillar crushing stage; **(d)** Integrated-interaction stage.

This four-stage evolutionary sequence demonstrates considerable spatiotemporal nonlinearity in stress transmission paths, energy dissipation processes, and surface deformation responses. Grasping this evolutionary mechanism is pivotal for long-term deformation prediction, optimized reinforcement scheme formulation, and systematic risk governance in analogous goaf–tunnel composite systems, while also furnishing a rigorous theoretical basis for regional land reclamation and the safe operation of critical infrastructure. Conversely, classical three-phase theories of mining-induced strata deformation (the "preparatory-active-decay" framework (Peng 1981; Zhou *et al.* 2023*a*; Chen and Wang 2025)) are primarily confined to immediate strata deformation responses during and short-term post-mining operations, exhibiting insufficient temporal scope to capture long-term delayed subsidence and inadequate mechanistic delineation of cascading roof-pillar failure processes. The proposed four-stage evolutionary model extends the temporal scope to delineate long-term (> 10 years) deformation dynamics and identifies cascading roof-pillar failure as the primary causal mechanism of post-mining settlement—representing

a scenario-specific refinement and extension of classical theories, thereby enhancing the scientific rigor of stability assessment for analogous engineering contexts.

5. Conclusion and future work

5.1. Conclusion

Drawing on comprehensive geological surveys, distress mapping and the spatial distribution of abandoned workings beneath the Taoping tunnel, this study combined time-series InSAR, the probability-integral method and high-resolution finite-element modelling to clarify the deformation processes of a railway tunnel undermined by longwall goaf. The key findings are as follows:

(1) InSAR deformation pattern: Surface subsidence is symmetric about the safety coal pillars and divides into five stages (2015–2024): quasi-stable → acceleration (2017–2018) → fluctuating deceleration (2018–2020) → second acceleration (2020–2023) → recent deceleration (2023–2024). Peak settlements coincide spatially with the flanking goaf zones; seasonal irrigation-induced consolidation amplifies mining subsidence.

(2) Mechanism revealed by numerical modelling: Mining reconfigures the stress field. At 150 m extraction length, roof tensile stress reaches its limit, triggering initial cantilever failure and downward migration of maximum tension to the floor. Beyond 350 m, floor tensile stress rises progressively, heralding floor instability. In contrast to conventional scenarios, this goaf experienced pronounced subsidence after mining had stopped. Post-mining subsidence is driven by progressive pillar crushing: stress redistribution concentrates compression in the pillar, exceeds its strength and causes progressive failure, leading to regional settlement.

(3) Ten-year PIM forecast: Settlement decays spatially from the goaf center and temporally by 10% per year, indicating rapid attenuation and entry into the residual stabilization phase, ensuring a safe basis for land reuse.

(4) Four-stage evolutionary model: Initial stability → roof rupture → pillar crushing → "Balance" type instability. Advancing panels first collapse the roof to form local bowls; load transfer then crushes the central pillars; ultimate pillar failure creates a symmetric, large-scale depression. This nonlinear roof–pillar cascading mechanism governs long-term surface deformation and provides a framework for stability assessment and targeted remediation of similar goaf–tunnel systems.

5.2. Limitations and future work

This study has inherent limitations that warrant recognition: time-series InSAR, a core monitoring technique, is subject to atmospheric delay errors and temporal decorrelation, introducing marginal uncertainties in 3D deformation quantification; the 2D finite-element model, while computationally efficient, neglects 3D spatio-temporal effects (e.g., 3D goaf distribution, lateral stress transmission, tunnel longitudinal deformation) and stratigraphic heterogeneity, compromising the accuracy of stress-deformation predictions; additionally, the proposed four-stage model and mechanisms are context-specific to the Taoping tunnel's geological-engineering setting, requiring validation across diverse scenarios to enhance generalizability.

To mitigate these limitations, future research will integrate multi-source monitoring (e.g., multi-track InSAR, GNSS) to reconstruct the complete 3D deformation field and reduce InSAR-related uncertainties, establish a 3D numerical model incorporating actual goaf geometry and tunnel longitudinal characteristics, conduct comparative studies in diverse goaf–tunnel systems to refine the evolutionary model, and combine in-situ stress-displacement monitoring with numerical simulations to validate the cascading failure mechanism, enhancing both theoretical rigor and engineering utility.

Data availability statement

The data or datasets that support the findings of this study are available from the corresponding author upon reasonable request.

Declaration of generative AI and AI-assisted technologies

During the preparation of this manuscript, the authors used generative AI tools only to improve language and readability. The authors take full responsibility for the content of the manuscript.

Acknowledgments

Funding: This study was partially funded by the Major Instrument Project of the National Natural Science Foundation of China (No. 42027806) and National Key Research and Development Program of China (No. 2023YFC3008404).

Authors' contribution

Conceptualization, H.M. and T.G.; methodology, H.M. and S.L.; software, H.M. and Y.T.; validation, T.G., B.C. and S.L.; formal analysis, H.M.; investigation, H.M., S.L. and R.F.; resources, H.M.; data curation, H.M., Y.T. and R.F.; writing—original draft preparation, H.M.; writing—review and editing, H.M., T.G., S.L. and B.C.; visualization, H.M.; supervision, T.G.; project administration, T.G.; funding acquisition, T.G. All authors have read and agreed to the published version of the manuscript.

Conflicts of interest

The authors declare no conflicts of interest.

References

Apanowicz B, Milczarek W, Kowalski A. Advanced InSAR-SBAS method for determining the extent of mining-induced deformations. *Geocarto Int.* 2025, 40(1):2523428. DOI: 10.1080/10106049.2025.2523428

Ashraf T, Yin F, Liu L, Zhang Q. Land subsidence detection using SBAS- and stacking-InSAR with zonal statistics and topographic correlations in Lakhra Coal Mines, Pakistan. *Remote Sens.* 2024, 16(20):3815. DOI: 10.3390/rs16203815

Chen X. Structural damage evolution and treatment strategies of the Taoping tunnel under mining-induced subsidence (In Chinese). *China Railway* 2025, 2025:44–53. DOI: 10.19549/j.issn.1001-683x.2024.05.27.003

Chen Y, Wang L. Robust parameter inversion of coal mining subsidence based on the combination of RANSAC and DE algorithms. *Sci. Rep.* 2025, 15(1):17283–17283. DOI: 10.1038/S41598-025-02103-X

Cong J, Hu Y, Fan G, Zhu Q, Liu D, *et al*. Exploring debris flow deposit morphology in river valleys: insights from physical modeling experiments. *Eng. Geol.* 2024, 332:107465. DOI: 10.1016/j.enggeo.2024.107465

Cui B, Gu T, Wang J, Li J, Fan N, *et al*. Analysis of seepage and hysteresis effect mechanism of un-saturated loess based on resistivity test. *J. Hydrol.* 2025, 653:132749. DOI: 10.1016/j.jhydrol.2025.132749

Declercq PY, Dusar M, Pirard E, Verbeurgt J, Choopani A, *et al*. Post mining ground deformations transition related to coal mines closure in the Campine Coal Basin, Belgium, evidenced by three decades of MT-InSAR data. *Remote Sens.* 2023, 15(3):725. DOI: 10.3390/rs15030725

Du W, Guo M, Lai J, Zhang Y, Ma Y, *et al*. Fitting analysis of the curve of main inclined section of surface subsidence of insufficient mining. *Front. Earth Sci.* 2025, 13:1525363. DOI: 10.3389/feart.2025.1525363

Duan J, Zheng J, Yang Y, Song Y, La A, *et al*. Design and analysis of photon imaging detector based on printed circuit board technology cross strip anode. *Appl. Sci.* 2023, 13(22):12304. DOI: 10.3390/app132212304

Dudek M, Sroka A, Tajduś K, Misa R, Mrocheń D. Assessment and duration of the surface subsidence after the end of mining operations. *Energies* 2022, 15(22):8711. DOI: 10.3390/en15228711

Fan H, Li T, Gao Y, Deng K, Wu H. Characteristics inversion of underground goaf based on InSAR techniques and PIM. *Int. J. Appl. Earth Obs. Geoinf.* 2021, 103:102526. DOI: .1016/j.jag.2021.102526

Gabriel AK, Goldstein RM, Zebker HA. Mapping small elevation changes over large areas: differential radar interferometry. *J. Geophys. Res. Solid Earth* 1989, 94:9183–9191. DOI: 10.1029/JB094iB07p09183

Gong J, Wang W, Li X, He W, Yuan Y, *et al*. Statistics of China's railway tunnels by the end of 2024 and overview of tunnels of new projects in 2024. *Tunnel Constr.* 2025, 45(3):636–653. DOI: 10.3973/j.issn.2096-4498.2025.03.019

Guo L, Hou K, Sun H, Yang Y. Stability evaluation of the goaf based on combination weighting and cloud model. *Adv. Civ. Eng.* 2024, 2024:6618372. DOI: 10.1155/2024/3884586

Hamza V, Stopar B, Sterle O, Pavlovčič-Prešeren P. Observations and positioning quality of low-cost GNSS receivers: a review. *GPS Solutions* 2024, 28:104. DOI: 10.1007/s10291-024-01686-8

He L, Wu D, Ma L. Numerical simulation and verification of goaf morphology evolution and surface subsidence in a mine. *Eng. Fail. Anal.* 2023, 144:106918. DOI: 10.1016/j.engfailanal.2022.106918

Herrera-García G, Ezquerro P, Tomás R, Béjar-Pizarro M, López-Vinielles J, *et al*. Mapping the global threat of land subsidence. *Science* 2021, 371:34–36. DOI: 10.1126/SCIENCE.ABB8549

Huang X, Li X, Li H, Duan S, Yang Y, *et al*. Study on the movement of overlying rock strata and surface movement in mine goaf under different treatment methods based on PS-InSAR technology. *Appl. Sci.* 2024, 14(6):2651. DOI: 10.3390/app14062651

Jeon B, Jeong H, Choi S, Jeon S. Assessment of subsidence hazard in abandoned mine area using strength reduction method. *KSCE J. Civ. Eng.* 2022, 26(10):4338–4358. DOI: 10.1007/s12205-022-2408-z

Jia H, Yan B, Guan K, Liu H, Wu Q, *et al*. Stability analysis of shallow goaf based on field monitoring and numerical simulation: a case study at an open-pit iron mine, China. *Front. Earth Sci.* 2022, 10:880410. DOI: 10.3389/FEART.2022.897779

Jiang Y, Misa R, Li P, Yuan X, Sroka A, *et al*. Review of the development history of mining subsidence theory (In Chinese). *Met. Mine* 2019, 10:1–7. DOI: 10.19614/j.cnki.jsks.201910001

Jing W, Zhao Y, Kong J, Huang C, Jilani KMK, *et al*. The time-space prediction model of surface settlement for above underground gas storage cavern in salt rock based on Gaussian function. *J. Nat. Gas Sci. Eng.* 2018, 53:45–54. DOI: 10.1016/j.jngse.2018.02.024

Kopeć A, Bugajska N, Milczarek W, Głąbicki D. Long-term monitoring of the impact of mining operations on the ground surface at the regional scale based on the InSAR-SBAS technique, the Upper Silesian Coal Basin (Poland). Case study. *Acta Geodyn. Geomater.* 2022, 19(1):93–110. https://doi.org/10.13168/AGG.2021.0044

Li J, Zang M, Xu N, Mei G, Yang S. An interferometric-synthetic-aperture-radar-based method for predicting long-term land subsidence in goafs through the concatenation of multiple sources of short-term monitoring data. *Remote Sens.* 2023, 15(17):4203. DOI: 10.3390/rs15174203

Li L. Surface deformation characteristics and disaster analysis of Taoping tunnel (In Chinese). *J. Railway Eng. Soc.* 2019, 36:66–72.

Li M, Li K, Liu Y, Wu S, Qin Q, *et al*. Goaf risk prediction based on IAOA–SVM and numerical simulation: a case study. *Underground Space* 2024, 15:153–175. DOI: 10.1016/J.UNDSP.2023.07.003

Li S, Yu L, Jiang W, Yu H, Wang X. The recent progress China has made in green mine construction, Part I: mining groundwater pollution and sustainable mining. *Int. J. Environ. Res. Public Health* 2022, 19(9):5673. DOI: 10.3390/ijerph19095673

Litwiniszyn J. Application of the equation of stochastic processes to mechanics of loose bodies. *Arch. Mech.* 1956, 8:393–411.

Liu B, Liao G. *Basic Laws of Surface Movement in Coal Mines (In Chinese)*. Beijing: China Industry Press, 1965.

Liu Y, Gu T, Wang Y, Xiong W, Yang X. Deformation characteristics of overlying strata in room and pillar mined-out areas under coal pillar instability. *Sci. Rep.* 2024, 14:1006. DOI: 10.1038/S41598-023-50996-3

Modeste G, Doubre C, Masson F. Time evolution of mining-related residual subsidence monitored over a 24-year period using InSAR in southern Alsace, France. *Int. J. Appl. Earth Obs. Geoinf.* 2021, 102:102392. DOI: 10.1016/J.JAG.2021.102392

Peng S. Coal mine ground control. *Eng. Geol.* 1981, 17(1,2):76,77. DOI: 10.1016/0013-7952(81)90030-2

Peng S, Qin S, Wang M, Li G. Mining subsidence prediction for multi-seam and non-rectangular goafs based on probability integral model: a case study from China. *Arab. J. Geosci.* 2021, 14:1279. DOI: 10.1007/s12517-021-07620-3

Przyłucka M, Kowalski Z, Perski Z. Twenty years of coal mining-induced subsidence in the Upper Silesia in Poland identified using InSAR. *Int. J. Coal. Sci. Technol.* 2022, 9:86. DOI: 10.1007/s40789-022-00541-w

Ren L, He P, Zou Y, Yang C, Dun Z, *et al*. A novel evaluation method of mining goaf ground activation under high-speed railway load. *Front. Earth Sci.* 2022, 10:852364. DOI: 10.3389/feart.2022.931466

Rigamonti S, Previati A, Dattola G, Crosta G B. Assessing twin tunnel-induced ground settlements in alluvial deposits by InSAR data. *Eng. Geol.* 2025, 352:108059. DOI: 10.1016/j.enggeo.2025.108059

Sakhno I, Sakhno S, Petrenko A, Barkova O, Kobylianskyi B. Numerical simulation of the surface subsidence evolution caused by the flooding of the longwall goaf during excavation of thin coal seams. *IOP Conf. Ser. Earth Environ. Sci.* 2023, 1254:012057. DOI: 10.1088/1755-1315/1254/1/012057

Salmi EF, Nazem M, Karakus M. The effect of rock mass gradual deterioration on the mechanism of post-mining subsidence over shallow abandoned coal mines. *Int. J. Rock Mech. Min. Sci.* 2017, 91:59–71. DOI: 10.1016/j.ijrmms.2016.11.012

Shi Z, Wang Q, Wang P, He D, Bai Y, *et al*. Time series effect on surface deformation above goaf area with multiple-seam mining. *Symmetry* 2020, 12(9):1428. DOI: 10.3390/sym12091428

Sidki-Rius N, Sanmiquel L, Bascompta M, Parcerisa D. Subsidence management and prediction system: a case study in potash mining. *Minerals* 2022, 12(9):1155. DOI: 10.3390/min12091155

Sun Y, Zuo J, Karakus M, Wang J. Investigation of movement and damage of integral overburden during shallow coal seam mining. *Int. J. Rock Mech. Min. Sci.* 2019, 117:63–75. DOI: 10.1016/j.ijrmms.2019.03.019

Teixeira AC, Bakon M, Perissin D, Sousa JJ. InSAR Analysis of partially coherent targets in a subsidence deformation: a case study of Maceió. *Remote Sens*. 2024, 16(20):3806. DOI: 10.3390/rs16203806

Tian H, Wang Y. Correlation analysis of tunnel diseases and mining subsidence based on InSAR: a case study of the Taoping tunnel (In Chinese). *Stand. Surv. Mapp*. 2022, 38(1):22–24. DOI: 10.20007/j.cnki.61-1275/P.2022.01.05

Wang F, Hu L, Hu Y. Study on the causes of defects in the Houyue Line Taoping tunnel and their treatment schemes (In Chinese). *Mod. Tunn. Technol.* 2019, 56:192–199,204. DOI: 10.13807/j.cnki.mtt.2019.01.028

Wang G, Wu Q, Li P, Cui X, Gong Y, *et al*. Mining subsidence prediction parameter inversion by combining GNSS and DInSAR deformation measurements. *IEEE Access* 2021, 9:89043–89054. DOI: 10.1109/access.2021.3089820

Wang H, Li K, Zhang J, Hong L, Chi H. Monitoring and analysis of ground surface settlement in mining clusters by SBAS-InSAR technology. *Sensors* 2022, 22(10):3711. DOI: 10.3390/s22103711

Wang X. Study on deformation behavior of the Taoping tunnel under widespread underlying goaf (In Chinese). *Railway Stand. Des.* 2025, 69:117–123,159 DOI: 10.13238/j.issn.1004-2954.202405310003

Wo X, Li G, Li J, Yang S, Lu Z, *et al*. The roof safety under large mining height working face: a numerical and theoretical study. *Minerals* 2022, 12(10):1217. DOI: 10.3390/min12101217

Xu Z, Xu W, Zhou P, Zhu Z, Zhao J, *et al*. Research on coal mine goaf restoration based on stability of overlying rocks and numerical simulation analysis: a case study of Jingmen Garden Expo Park. *Sustainability* 2023, 15(2):1464. DOI: 10.3390/su15021464

Yang Y, Zhang M, Hu G, Guan K. Simulations of goaf surface subsidence via filling control. *PLoS One* 2022, 17:e0261740. DOI: 10.1371/journal.pone.0261740

Yuan X, Li X, Li X, Su T, Du H, *et al*. Multi-factor analysis and graded remediation strategy for goaf stability in underground metal mines: Fluid–solid coupling simulation and genetic algorithm-based optimization approach. *Symmetry* 2025, 17(7):1024. DOI: 10.3390/sym17071024

Yulaikhah Y, Pramumijoyo S, Widjajanti N. The effect of baseline component correlation on the design of GNSS network configuration for Sermo reservoir deformation monitoring. *Indones. J. Geogr.* 2019, 51:199–206. DOI: 10.22146/ijg.44914

Zhang F. Hydrogeological conditions and mine water filling characteristics of Yonghong Coal Mine (In Chinese). *Shaanxi Coal* 2009, 28:64,70,71.

Zhang F, Gu T, Kong J, Sun J. Soil-moisture variation in the Heifangtai slope under irrigation and rainfall based on the HYDRUS model (In Chinese). *J. Arid Land Resour. Environ.* 2021, 35(6):110–116 DOI: 10.13448/j.cnki.jalre.2021.165

Zhang H, Zhang J, Xu Z, Zhang J, Du S, *et al*. Overburden breakage and surface damage evolution under high-intensity mining of shallow coal seams: evidence from Shendong mining area. *Sci. Rep.* 2025, 15:5748. DOI: 10.1038/s41598-025-05177-9

Zhang S, Xu L, Long R, Chen L, Wang S, *et al*. Quantitative assessment and impact analysis of land surface deformation in Wuxi based on PS-InSAR and GARCH model. *Remote Sens.* 2024, 16(9):1568. DOI: 10.3390/rs16091568

Zhang X, Li W, Li T, Li Z, Cai G, *et al*. Stability analysis and numerical simulation of foundation in old goaf under building load. *Front. Earth Sci.* 2023, 11:1151684. DOI: 10.3389/FEART.2023.1063684

Zhou B, Yan Y, Kang J. Dynamic prediction model for progressive surface subsidence based on MMF time function. *Appl. Sci.* 2023, 13(14):8066. DOI: 10.3390/app13148066

Zhou B, Li S, Kang J, Zhang L, Zhang J, *et al*. A probability integral method modified model for accurately characterizing subsidence at the boundary of a mining area. *Sci. Rep*. 2025, 15:21014. DOI: 10.1038/s41598-025-05520-0

Zhou S, Wang H, Shan C, Liu H, Li Y, *et al*. Dynamic monitoring and analysis of mining land subsidence in multiple coal seams in the Ehuobulake Coal Mine based on FLAC3D and SBAS-InSAR technology. *Appl. Sci.* 2023, 13(15):8804. DOI: 10.3390/APP13158804

Zhu M, Yu X, Tan H, Yuan J. Integrated high-precision monitoring method for surface subsidence in mining areas using D-InSAR, SBAS, and UAV technologies. *Sci. Rep.* 2024a, 14:8465. DOI: 10.1038/s41598-024-63400-5

Zhu M, Yu X, Tan H, Yuan J, Chen K, *et al*. High-precision monitoring and prediction of mining area surface subsidence using SBAS-InSAR and CNN-BiGRU-attention model. *Sci. Rep.* 2024b, 14:13321. DOI: 10.1038/s41598-024-80446-7

Zhu N, Guo G, Li H, Wang T, Wang X. Prediction and analysis of surface residual deformation considering the impact of groundwater in mines. *Sustainability* 2024c, 16(19):8682. DOI: 10.3390/su16198682